

Precise determination of critical points of topological phase transitions via shift current in two-dimensional inversion asymmetric insulators

Zhongbo Yan^{1,*}

¹*School of Physics, Sun Yat-Sen University, Guangzhou 510275, China*

The precise determination of critical point is the basis to extract various critical properties of phase transitions. We identify that for two-dimensional inversion asymmetric insulators, with and without time-reversal symmetry, when topological phase transitions take place, all nonvanishing components of band-edge shift current tensor will reverse their signs in a singular way, regardless of what realistic value the temperature takes. This remarkable sign-reversal behavior of band-edge shift current tensor thus can be applied to determine the critical points of various topological phase transitions precisely, even for temperature-driven ones. We suggest concrete materials to test our predictions.

Since the first successful exfoliation of graphene[1], the family of two-dimensional (2D) materials has grown extremely fast over the last decade, ranging from insulators, metals to superconductors[2–4]. Owing to their atomically thin structures, 2D materials have demonstrated various novel phases, as well as fascinating electronic, optical and mechanical properties that do not exist in their bulk counterparts[4–8]. Another remarkable common feature of 2D materials is that their atomically thin structures also provide exceptional flexibility to tailor their bulk properties[9–13], suggesting that 2D materials are ideally suited for an in-depth investigation of various competing phases, as well as their transitions and critical properties[14, 15]. The emerged 2D materials also open up a new door for topological phases and related physics[16–18]. The most notable example is the demonstration of a quantum spin Hall insulating phase in graphene with intrinsic spin-orbit coupling[19, 20]. This conceptual breakthrough reveals that seemingly featureless band insulators actually have very rich physics and need to be further classified according to their underlying band topology[20–33]

The existence of distinct topological phases in insulators raises a natural question: what kind of new critical properties may emerge at the critical points of continuous topological phase transitions (TPTs) between distinct insulating phases. While the critical properties of TPTs have been actively studied in theory[34–43], thus far they have been largely unexplored in experiments, mainly owing to the lack of experimental methods that are able to determine the critical points of TPTs precisely. As is known, the critical points of conventional continuous phase transitions can simply be determined in experiments by the observation of singular behavior in physical quantities. For TPTs, as the name suggests, the most dramatic change are topological invariants, which, however, are not physical observables. Generally, the topological invariant of an insulating phase is revealed by measurements of quantized linear-response transport coefficients[44–47], however, owing to finite temperature effect and various scattering effects, the quantization of linear-response transport coefficients breaks down when the system gets closed to the critical point at which the band gap vanishes, indicating the absence of any singular signature in these observables at the critical point[48].

In this work, we show that a measurement of shift current (a nonlinear optical effect[49–51]) can determine the critical points of TPTs in 2D inversion asymmetric insulators precisely, owing to that the band-edge shift current tensor will display a singular sign-reversal behavior across the critical points. As is known, only two of the ten symmetry classes, class AII (with time-reversal symmetry (TRS)) and class A (without TRS), can host topological insulating phases in 2D[26, 27]. The former is classified by a Z_2 number, while the latter is classified by an integer, the Chern number[26, 27]. Remarkably, we demonstrate compactly that in the absence of inversion symmetry (a prerequisite for the presence of shift current[49–51]), all nonvanishing components of band-edge shift current tensor will reverse their signs in a singular way across the TPTs allowed by these two symmetry classes, regardless of what realistic value the temperature takes, indicating the wide applicability of this approach in 2D. Noteworthy, while in the absence of inversion symmetry certain component of shift current tensor was also found to reverse its sign when a normal insulator is transitioned to a topological insulator in 3D[52], the transition itself is in general indirect owing to the existence of an intermediate gapless phase[53, 54].

General theory.— Near the critical point of a continuous TPT, the relevant physics are faithfully described by the low-energy Hamiltonian around the band edge with the smallest energy gap. For generality, we consider the low-energy Hamiltonian takes the form $H = \sum_{q;\alpha} \Psi_{\alpha;\mathbf{q}}^\dagger H_\alpha(\mathbf{q}) \Psi_{\alpha;\mathbf{q}}$ with $\Psi_\alpha = (c_{\alpha;\mathbf{q};1}, \dots, c_{\alpha;\mathbf{q};n})^T$ an n -component spinor, α labeling the α -th band edge, and $\mathbf{q} = (q_x, q_y)$ the momentum relative to the band edge. Different $H_\alpha(\mathbf{q})$ are related by symmetry, so that they are degenerate in energy and their energy gaps get closed and reopened at the same time.

For 2D inversion asymmetric insulators without TRS, the low-energy Hamiltonian is in general a rank-2 matrix. The presence of TRS in general requires it to be a rank-4 matrix, but if spin conserves, it can be reduced as the direct sum of two rank-2 matrices. For simplicity, we first confine ourselves to the spin conserving case if TRS is respected and address the spin non-conserving case later. Then to second order in momentum, the general form of $H_\alpha(\mathbf{q})$ is $H_\alpha(\mathbf{q}) = \mathbf{d}_\alpha(\mathbf{q}) \cdot$

$\tau + \epsilon_\alpha(\mathbf{q})\mathbf{I}$, with

$$\begin{aligned} d_{\alpha;x}(\mathbf{q}) &= \Delta_{\alpha;x} + v_{\alpha;x}q_x + A_{\alpha;ij}q_iq_j, \\ d_{\alpha;y}(\mathbf{q}) &= \Delta_{\alpha;y} + v_{\alpha;y}q_y + B_{\alpha;ij}q_iq_j, \\ d_{\alpha;z}(\mathbf{q}) &= m_\alpha + \lambda_{\alpha;x}q_x + \lambda_{\alpha;y}q_y + C_{\alpha;ij}q_iq_j, \end{aligned} \quad (1)$$

$\tau = (\tau_x, \tau_y, \tau_z)$ the Pauli matrices, and \mathbf{I} the rank-2 unit matrix. We will set $\epsilon_\alpha(\mathbf{q}) = 0$ below, since it is irrelevant to the physics we will discuss. The parameters $\{\Delta_{\alpha;x,y}, m_\alpha, v_{\alpha;x,y}, \lambda_{\alpha;x,y}, A_{\alpha;ij}, B_{\alpha;ij}, C_{\alpha;ij}\}$ are all momentum-independent, and $X_{ij}q_iq_j$ with $X = \{A, B, C\}$ is a shorthand notation of $X_{xx}q_x^2 + X_{yy}q_y^2 + X_{xy}q_xq_y$. To ensure that the Hamiltonian correctly describes the band edge, all linear momentum terms in the energy spectra ($E_\alpha^\pm = \pm d_\alpha$, with $d_\alpha \equiv \sqrt{d_{\alpha;x}^2 + d_{\alpha;y}^2 + d_{\alpha;z}^2}$) must vanish, which puts the following two constraints on the above parameters,

$$\Delta_{\alpha;x}v_{\alpha;x} = -m_\alpha\lambda_{\alpha;x}, \quad \Delta_{\alpha;y}v_{\alpha;y} = -m_\alpha\lambda_{\alpha;y}. \quad (2)$$

Topological properties of $H_\alpha(\mathbf{q})$ are characterized by the Chern number[55] (note if TRS is preserved, H_α has a TRS partner with opposite Chern number, and the total Hamiltonian H is characterized by a Z_2 number). Neglect all quadratic momentum terms in $H_\alpha(\mathbf{q})$, a short calculation reveals that the Chern number $C_\alpha = \frac{1}{2}\text{sgn}(v_{\alpha;x}v_{\alpha;y}m_\alpha)$, indicating that $H_\alpha(\mathbf{q})$ will undergo a TPT when the mass term m_α changes sign. As in general the coefficients of the terms containing momentum will keep their signs when m_α is varied across the critical point, the constraints in Eq.(2) indicate that as long as $\Delta_{\alpha;x}$ and $\Delta_{\alpha;y}$ do not identically equal zero

($\Delta_\alpha \equiv 0$ implies $\lambda_\alpha \equiv 0$), they will change their signs with m_α at the same time.

Let us now investigate the shift current, which is a second-order optical effect with the induced direct current proportional to the square of optical field[49–51, 56–64]), i.e., $J_a = \sigma_\alpha^{abb}(\omega)\mathcal{E}_b(\omega)\mathcal{E}_b(-\omega)$, where σ_α^{abb} represents the shift current tensor, and \mathcal{E}_b denotes the optical field. For the two-band Hamiltonian $H_\alpha(\mathbf{q})$, the shift current tensor is simply determined by the following formula[51, 56, 65]

$$\sigma_\alpha^{abb}(\omega) = \frac{4\pi e^3}{\hbar^4 \omega^3} \int \frac{d^2q}{(2\pi)^2} [F_{1\alpha}^{abb} + F_{2\alpha}^{abb}] f_\alpha^{-+} \delta(\hbar\omega - 2d_\alpha) \quad (3)$$

where $a, b = \{x, y\}$, $f_\alpha^{-+} = f(-d_\alpha) - f(d_\alpha)$, with $f(d_\alpha) = 1/\{1 + \exp[(d_\alpha - \mu)/k_B T]\}$ the Fermi-Dirac distribution function (μ the chemical potential, T the temperature, and k_B the Boltzmann constant). Expressions for the two integrands in bracket are $F_{1\alpha}^{abb} = \mathbf{d}_\alpha \cdot (\partial_{ab}\mathbf{d}_\alpha \times \partial_b\mathbf{d}_\alpha)$ and $F_{2\alpha}^{abb} = (\hbar\omega)^2 \Omega_{\alpha;ab} \partial_b d_\alpha / 2$, with $\Omega_{\alpha;ab} = -\mathbf{d}_\alpha \cdot (\partial_a\mathbf{d}_\alpha \times \partial_b\mathbf{d}_\alpha) / 2d_\alpha^3$ the Berry curvature of the valence band[55]. Because $\Omega_{\alpha;ab}$ vanishes identically when $a = b$, it is readily seen that $F_{2\alpha}^{xxx}$ and $F_{2\alpha}^{yyy}$ also vanish identically. For $F_{2\alpha}^{xyy}$ and $F_{2\alpha}^{yxx}$, because $\partial_b d_\alpha$ vanishes at the band edge, this indicates that they also do not contribute to the shift current tensor when the optical frequency exactly matches the band gap, i.e., $\omega = E_{g;\alpha} \equiv 2\min\{d_\alpha\} = 2\sqrt{\Delta_{\alpha;x}^2 + \Delta_{\alpha;y}^2 + m_\alpha^2}$. Near the band edge, leading order terms of $F_{2\alpha}^{xyy}$ and $F_{2\alpha}^{yxx}$ are found to be linear in momentum, thus their contributions can be safely neglected in this regime. For $F_{1\alpha}^{abb}$, a straightforward calculation reveals $F_{1\alpha}^{abb} = F_{1\alpha}^{abb(0)} + \mathcal{O}(\mathbf{q})$, where $F_{1\alpha}^{abb(0)}$ represents the zeroth-order term in momentum and

$$\begin{aligned} F_{1\alpha}^{xxx(0)} &= (\Delta_{\alpha;x}\lambda_{\alpha;x} - m_\alpha v_{\alpha;x})B_{\alpha;xx} + \Delta_{\alpha;y}(C_{\alpha;xx}v_{\alpha;x} - A_{\alpha;xx}\lambda_x), \\ F_{1\alpha}^{yyy(0)} &= (m_\alpha v_{\alpha;y} - \Delta_{\alpha;y}\lambda_{\alpha;y})A_{\alpha;yy} + \Delta_{\alpha;x}(B_{\alpha;yy}\lambda_{\alpha;y} - C_{\alpha;yy}v_{\alpha;y}), \\ F_{1\alpha}^{yxx(0)} &= (\Delta_{\alpha;x}\lambda_{\alpha;x} - m_\alpha v_{\alpha;x})B_{\alpha;xy} + \Delta_{\alpha;y}(C_{\alpha;xy}v_{\alpha;x} - A_{\alpha;xy}\lambda_{\alpha;x}), \\ F_{1\alpha}^{xyy(0)} &= (m_\alpha v_{\alpha;y} - \Delta_{\alpha;y}\lambda_{\alpha;y})A_{\alpha;xy} + \Delta_{\alpha;x}(B_{\alpha;xy}\lambda_{\alpha;y} - C_{\alpha;xy}v_{\alpha;y}). \end{aligned} \quad (4)$$

As $\Delta_{\alpha;x}$, $\Delta_{\alpha;y}$ and m_α change their signs simultaneously, it is readily seen that all components of $F_{1\alpha}^{abb(0)}$ will reverse their signs across the critical point.

Applying the formula in Eq.(3), we find that for optical frequency close to the band gap ($\mu = 0$ in this work),

$$\sigma_\alpha^{abb}(\omega) \simeq -\frac{e^3 F_{1\alpha}^{abb(0)}}{2\hbar^3 \omega^2 \bar{v}_\alpha} \tanh \frac{\hbar\omega}{4k_B T} \Theta(\hbar\omega - E_{g;\alpha}), \quad (5)$$

where $\bar{v}_\alpha = \sqrt{v_{\alpha;x}^2 v_{\alpha;y}^2 + \lambda_{\alpha;x}^2 v_{\alpha;y}^2 + v_{\alpha;x}^2 \lambda_{\alpha;y}^2}$, and $\Theta(x)$ is the Heaviside step function. For the convenience of discussion, we name $\sigma_\alpha^{abb}(\omega)$ with $\omega = E_{g;\alpha}$ *band-edge shift current tensor*. Two remarkable features of the band-edge shift current tensor can immediately be read from Eq.(5): (i) No

matter what realistic value the temperature takes, all nonvanishing components will reverse their signs across the TPT; (ii) All nonvanishing components have a discontinuous jump across the TPT, with the discontinuous jump inversely proportional to the temperature, and going divergent in the zero-temperature limit. Apparently, the singular sign-reversal behavior of band-edge shift current tensor can be easily detected in experiments, thus it can be applied as a sensitive approach to determine the critical points of TPTs, even for the class of TPTs driven by temperature[66–70]. Noteworthy, although here $H_\alpha(\mathbf{q})$ only describes TPTs with Chern number jump $|\Delta C_\alpha| = 1$, the singular sign-reversal behavior also appears for more unusual ones with $|\Delta C_\alpha| \geq 2$ as nonvanishing band-edge shift current tensor must be proportional to the zeroth-order

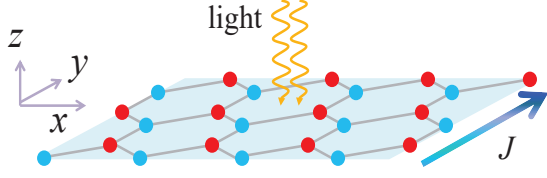


FIG. 1. A schematic of the honeycomb-lattice system. Without inversion symmetry, a photocurrent will be generated when a beam of linearly polarized light is incident perpendicular to the lattice plane.

der momentum terms in the low-energy Hamiltonian, which, as we have analyzed above, will change their signs across the TPT. Therefore, in the absence of inversion symmetry, the singular sign-reversal behavior is expected to hold for various TPTs allowed by class A in 2D.

As $H_\alpha(\mathbf{q})$ may have symmetry-related partners, let us analyze the effects of the allowed symmetries to the shift current tensor. In this work, for spatial symmetries, we confine ourselves to the symmorphic ones for simplicity and leave the more complicated nonsymmorphic symmetries for future study. Clearly, in 2D the absence of inversion symmetry directly rules out the C_2 , C_4 and C_6 rotation symmetry, as well as the existence of two mirror symmetries with respect to two orthogonal mirror planes. Therefore, 2D inversion asymmetric insulators can at most simultaneously have C_3 rotation symmetry, TRS and certain mirror symmetries whose mirror planes are not orthogonal. Clearly, shift current tensors from the band edges related by C_3 rotation symmetry have to be equal. Further analysis according to Eqs.(1) and (3) reveals that shift current tensors from the band edges related by TRS are equal, but are opposite for mirror symmetry. Since the effect of TRS is a doubling of shift current tensors, it becomes clear that the singular sign-reversal behavior of band-edge shift current tensor also holds for TPTs allowed by class AII in 2D.

Concrete model.— In the following we take the Kane-Mele model as a concrete example to demonstrate the above general analysis. A schematic diagram of the system is presented in Fig.1. The Hamiltonian reads[19, 20]

$$H = t \sum_{\langle ij \rangle} c_i^\dagger c_j + i\lambda_{\text{so}} \sum_{\langle\langle ij \rangle\rangle} \nu_{ij} c_i^\dagger s^z c_j + \lambda_v \sum_i \xi_i c_i^\dagger c_i, \quad (6)$$

in which the three terms in sequence refer to the nearest-neighbour hopping, spin-orbit coupling and stagger potential ($\xi_i = 1(-1)$ if $i \in A(B)$ sublattices) on a honeycomb lattice, respectively. The spin-orbit coupling is related to the second-nearest-neighbour hopping, and when the hopping trajectory is anticlockwise (clockwise), $\nu_{ij} = 1(-1)$. The presence of stagger potential breaks the crucial inversion symmetry.

In momentum space, $H = \sum_{\mathbf{k}} c_{\mathbf{k}}^\dagger H(\mathbf{k}) c_{\mathbf{k}}$ with $c_{\mathbf{k}} =$

$$(c_{A,\mathbf{k}\uparrow}, c_{B,\mathbf{k}\uparrow}, c_{A,\mathbf{k}\downarrow}, c_{B,\mathbf{k}\downarrow})^T \text{ and}$$

$$H(\mathbf{k}) = 2\lambda_{\text{so}} \left(2 \sin \frac{\sqrt{3}k_x a}{2} \cos \frac{3k_y a}{2} - \sin \sqrt{3}k_x a \right) \tau_z s_z \\ + \lambda_v \tau_z + t \left(\cos k_y a + 2 \cos \frac{\sqrt{3}k_x a}{2} \cos \frac{k_y a}{2} \right) \tau_x \\ + t \left(\sin k_y a - 2 \cos \frac{\sqrt{3}k_x a}{2} \sin \frac{k_y a}{2} \right) \tau_y, \quad (7)$$

where τ_i with $i = \{x, y, z\}$ are Pauli matrices acting on the sublattice space, and s_z is a Pauli matrix acting on the spin space. For brevity of notation, below we set the lattice constant $a = 1$ unless otherwise specified. It is easy to check that a $2\pi/3$ rotation of the momentum, $(k_x, k_y) \rightarrow (-k_x + \sqrt{3}k_y, -\sqrt{3}k_x - k_y)/2$, leaves the Hamiltonian intact, indicating the existence of C_3 rotation symmetry. The Hamiltonian is also invariant under time-reversal operation and mirror reflection about the $k_x = 0$ plane, i.e., $\mathcal{T}H(\mathbf{k})\mathcal{T}^{-1} = H(-\mathbf{k})$, $\mathcal{M}H(k_x, k_y)\mathcal{M}^{-1} = H(-k_x, k_y)$, with the time-reversal operator $\mathcal{T} = i s_y \mathcal{K}$ (\mathcal{K} the complex conjugate operator) and the mirror reflection operator $\mathcal{M} = s_x$.

The Kane-Mele model belongs to class AII and is well-known to host two topologically distinct phases (Z_2 classification)[19, 20]. For $|\lambda_v| < |\sqrt{3}\lambda_{\text{so}}|$, the model describes a quantum spin Hall insulator (or say topological insulator) with helical gapless modes on the boundary, while for $|\lambda_v| > |\sqrt{3}\lambda_{\text{so}}|$, it describes a normal insulator without gapless boundary modes. $|\lambda_v| = |\sqrt{3}\lambda_{\text{so}}|$ is the critical point at which the band gap is closed and TPT takes place.

As in this work the band-edge shift current tensor is of central interest, below we also focus on the low-energy Hamiltonian around the band edge at first. The band edges of this model are located at the two valleys $\mathbf{K} = (-4\pi/3\sqrt{3}, 0)$ and $\mathbf{K}' = (4\pi/3\sqrt{3}, 0)$. A short calculation reveals that the low-energy Hamiltonian is given by $H = \sum_{\chi, s; \mathbf{q}} \Psi_{\chi, s; \mathbf{q}}^\dagger H_{\chi, s}(\mathbf{q}) \Psi_{\chi, s; \mathbf{q}}$, where $\Psi_{\chi, s; \mathbf{q}} = (c_{A, \mathbf{q}, s}, c_{B, \mathbf{q}, s})^T$ and $H_{\alpha, s}(\mathbf{q}) = \mathbf{d}_{\chi, s}(\mathbf{q}) \cdot \boldsymbol{\tau}$ with

$$d_{\chi, s; x}(\mathbf{q}) = \frac{3t}{2} (\chi q_x + \frac{1}{4} q_x^2 - \frac{1}{4} q_y^2), \\ d_{\chi, s; y}(\mathbf{q}) = \frac{3t}{2} (q_y - \frac{1}{2} \chi q_x q_y), \\ d_{\chi, s; z}(\mathbf{q}) = m_{\chi, s} + \frac{9\sqrt{3}}{4} \lambda_{\text{so}} \chi s (q_x^2 + q_y^2), \quad (8)$$

where $\chi = 1(-1)$ for $K(K')$ valley, and $s = 1(-1)$ for up(down) spin. $m_{\chi, s} = -3\sqrt{3}\lambda_{\text{so}}\chi s + \lambda_v$ denotes the Dirac mass. Following Eqs.(3) and 4, we find $\sigma_{\chi, s}^{xxx}$ and $\sigma_{\chi, s}^{xyy}$ vanish identically for every choice of (χ, s) , thus $\sigma^{xxx} = \sum_{\chi, s} \sigma_{\chi, s}^{xxx}$ and $\sigma^{xyy} = \sum_{\chi, s} \sigma_{\chi, s}^{xyy}$ are both equal to zero, consistent with the fact that the full Hamiltonian is mirror symmetric about the $k_x = 0$ plane. For the remaining two components, we find that for optical frequency close to the band gap[65],

$$\sigma_{\chi, s}^{yyy}(\omega) \simeq -\frac{e^3 a m_{\chi, s}}{4\hbar^3 \eta_{\chi, s} \omega^2} \tanh \frac{\hbar\omega}{4k_B T} \Theta(\hbar\omega - 2|m_{\chi, s}|), \\ \sigma_{\chi, s}^{yxx}(\omega) \simeq \frac{e^3 a m_{\chi, s}}{4\hbar^3 \eta_{\chi, s} \omega^2} \tanh \frac{\hbar\omega}{4k_B T} \Theta(\hbar\omega - 2|m_{\chi, s}|), \quad (9)$$

where $\eta_{\chi,s} = 1 + 2\sqrt{3}\lambda_{\text{so}}m_{\chi,s}\chi s/t^2$ is a dimensionless quantity. We have restored the lattice constant based on dimensional analysis. Once $\lambda_v \neq 0$, $\sigma^{yyy} = \sum_{\chi,s} \sigma_{\chi,s}^{yyy}$ and $\sigma^{yxx} = \sum_{\chi,s} \sigma_{\chi,s}^{yxx}$ will take a finite value for optical frequency above the band gap. For the general case with finite λ_{so} and λ_v , the Dirac mass $m_{\chi,s}$ will have two different values, and only the two contributions related to the smaller Dirac mass are relevant to band edges. For the convenience of discussion, below we consider both λ_{so} and λ_v are positive, then the smaller Dirac mass takes the value $\lambda_v - 3\sqrt{3}\lambda_{\text{so}}$. For frequency exactly matching the band gap, it is straightforward to find

$$\begin{aligned}\sigma^{yyy}(\omega = 2|m|) &= -\frac{e^3 a}{8\hbar\eta m} \tanh \frac{|m|}{2k_B T}, \\ \sigma^{yxx}(\omega = 2|m|) &= \frac{e^3 a}{8\hbar\eta m} \tanh \frac{|m|}{2k_B T},\end{aligned}\quad (10)$$

where $m = \lambda_v - 3\sqrt{3}\lambda_{\text{so}}$, and $\eta = 1 + 2\sqrt{3}\lambda_{\text{so}}m/t^2$. Results clearly demonstrate that the band-edge shift current tensors, so too the band-edge shift current, will reverse their signs in a singular way across the TPT. It is noteworthy that if only one spin degree of freedom is considered, the Kane-Mele model reduces to the Haldane model (belongs to class A) in which TRS is absent and the TPTs are between a quantum anomalous Hall insulator (or say Chern insulator) with Chern number $|C| = 1$ and a normal insulator with $C = 0$ [71]. Apparently, the singular sign-reversal behavior of band-edge shift current tensor holds for the TPTs of the Haldane model.

Before ending this section, let us give further discussions on the shift current of this concrete model. As only σ^{yyy} and σ^{yxx} take nonzero values when the optical frequency is above the band gap, the shift current will be generated along the y direction when a beam of linearly polarized light is incident perpendicular to the system, as illustrated in Fig.1. Furthermore, as $\sigma^{yyy} \simeq -\sigma^{yxx}$, the sign difference provides a knob to tune the strength and direction of the shift current through the polarization of the light, potentially allowing novel applications in optoelectronics. Interestingly, when the polarization is bound in the x direction, the shift current is purely a nonlinear Hall current, i.e., the current flows in the direction perpendicular to the optical field. As is originated from interband processes, this nonlinear Hall effect is distinct from the one induced by Berry curvature dipole[72–74] which is an intraband effect.

For completeness, Fig.2 presents the shift current tensor of the full Hamiltonian (7). As we found that $\sigma^{yyy} \simeq -\sigma^{yxx}$ holds even for frequency much larger than the band gap, here only σ^{yyy} is presented. The result clearly demonstrates the sign-reversal behavior of band-edge shift current tensor across the TPT. Furthermore, we also verified numerically that the introduction of Rashba spin-orbit coupling to the Kane-Mele model, which keeps the TRS but breaks the spin conservation, does not change the sign-reversal behavior[65], indicating that this remarkable behavior holds no matter whether the spin conserves or not.

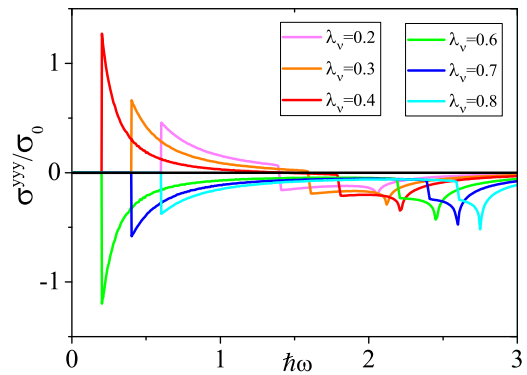


FIG. 2. The nonvanishing longitudinal component of shift current tensor for the Kane-Mele model. We set $t = 1$ as the energy unit, other parameters are: $\lambda_{\text{so}} = \sqrt{3}/18$, $\sigma_0 = (e^3 a/\hbar) \tanh(\hbar\omega/4k_B T)$. For the parameters chosen, $\lambda_v = 0.5$ is a critical point of TPT. The sign-reversal behavior of band-edge shift current tensor associated with TPT is clearly seen.

Experimental considerations and conclusions.— Though the relevance to many 2D inversion asymmetric materials[16–18], here we suggest two classes of materials to test our predictions. The first class of materials are monolayer group-IV elements, including silicene[75, 76], germanene[75, 76], stanene[77], and their alloys, whose underlying topological properties are described by the very Kane-Mele model. Owing to their buckled structures, their band gaps can be continuously tuned by gate voltage[12, 13, 78] or strain[79], thus continuous TPTs in this class of materials can be achieved. The second class of materials are structural inversion asymmetric quantum wells. Noteworthy, it has been experimentally confirmed that for sufficient thickness, the AlSb/InAs/GaSb/AlSb quantum well is a small gap topological insulator[80]. For this quantum well, TPT can also be continuously tuned by gate voltage[81], thus our proposal can immediately be tested.

The shift current can be detected by short-circuit current measurements[50, 82, 83]. While tracking the evolution of band-edge shift current tensor across TPTs can irrefutably determine the critical points, in experiments it is more practical to keep the frequency of optical field fixed at a sufficiently small value, and detect the sign-reversal behavior of shift current only. As an estimation, we consider the frequency $\hbar\omega = 1$ meV, the field strength $\mathcal{E} = 10^5$ V/m, the temperature $T = 10$ K, the lattice constant $a = 4\text{\AA}$, and a change of Dirac mass from $m = 0.01$ meV to -0.01 meV, then according to Eq.(9), it is readily found that the shift current will change from $J \sim 0.1$ A/cm to -0.1 A/cm. Such a notable sign-reversal behavior can be easily detected in experiments.

In conclusion, we have demonstrated that for 2D inversion asymmetric insulators, with and without TRS, a measurement of shift current can determine the critical points of various TPTs precisely, even for temperature-driven ones[66–70], hopefully paving the way for future research on 2D TPTs. This work may also stimulate studies of other nonlinear effects across TPTs, as well as further exploration of the effects

of interaction and disorder to such nonlinear effects.

Acknowledgements.— The author would like to thank Shuai Yin and Wen Huang for helpful suggestions on the manuscript. The author would also like to acknowledge the support by a startup grant at Sun Yat-sen University, and express his thanks to Institute for Advanced Study, Tsinghua University, where partial of this work was done.

* yanzhb5@mail.sysu.edu.cn

- [1] K. S. Novoselov, A. K. Geim, S. V. Morozov, D. Jiang, Y. Zhang, S. V. Dubonos, I. V. Grigorieva, and A. A. Firsov, “Electric field effect in atomically thin carbon films,” *Science* **306**, 666–669 (2004).
- [2] Pere Miró, Marsha Audiffred, and Thomas Heine, “An atlas of two-dimensional materials,” *Chem. Soc. Rev.* **43**, 6537–6554 (2014).
- [3] K. S. Novoselov, A. Mishchenko, A. Carvalho, and A. H. Castro Neto, “2d materials and van der waals heterostructures,” *Science* **353** (2016), 10.1126/science.aac9439.
- [4] Qing Hua Wang, Kourosh Kalantar-Zadeh, Andras Kis, Jonathan N. Coleman, and Michael S. Strano, “Electronics and optoelectronics of two-dimensional transition metal dichalcogenides,” *Nature Nanotechnology* **7**, 699 (2012).
- [5] A. K. Geim and I. V. Grigorieva, “Van der waals heterostructures,” *Nature* **499**, 419 (2013).
- [6] Sheneve Z. Butler, Shawna M. Hollen, Linyou Cao, Yi Cui, Jay A. Gupta, Humberto R. Gutierrez, Tony F. Heinz, Seung Sae Hong, Jiaying Huang, Ariel F. Ismach, Ezekiel Johnston-Halperin, Masaru Kuno, Vladimir V. Plashnitsa, Richard D. Robinson, Rodney S. Ruoff, Sayeef Salahuddin, Jie Shan, Li Shi, Michael G. Spencer, Mauricio Terrones, Wolfgang Windl, and Joshua E. Goldberger, “Progress, challenges, and opportunities in two-dimensional materials beyond graphene,” *ACS Nano* **7**, 2898 (2013).
- [7] Fengnian Xia, Han Wang, Di Xiao, Madan Dubey, and Ashwin Ramasubramanian, “Two-dimensional material nanophotonics,” *Nature Photonics* **8**, 899 (2014).
- [8] Gianluca Fiori, Francesco Bonaccorso, Giuseppe Iannaccone, Tomás Palacios, Daniel Neumaier, Alan Seabaugh, Sanjay K. Banerjee, and Luigi Colombo, “Electronics based on two-dimensional materials,” *Nature Nanotechnology* **9**, 768 (2014).
- [9] Eduardo V. Castro, K. S. Novoselov, S. V. Morozov, N. M. R. Peres, J. M. B. Lopes dos Santos, Johan Nilsson, F. Guinea, A. K. Geim, and A. H. Castro Neto, “Biased bilayer graphene: Semiconductor with a gap tunable by the electric field effect,” *Phys. Rev. Lett.* **99**, 216802 (2007).
- [10] Gui Gui, Jin Li, and Jianxin Zhong, “Band structure engineering of graphene by strain: First-principles calculations,” *Phys. Rev. B* **78**, 075435 (2008).
- [11] Kin Fai Mak, Chun Hung Lui, Jie Shan, and Tony F. Heinz, “Observation of an electric-field-induced band gap in bilayer graphene by infrared spectroscopy,” *Phys. Rev. Lett.* **102**, 256405 (2009).
- [12] Zeyuan Ni, Qihang Liu, Kechao Tang, Jiabin Zheng, Jing Zhou, Rui Qin, Zhengxiang Gao, Dapeng Yu, and Jing Lu, “Tunable bandgap in silicene and germanene,” *Nano Lett.* **12**, 113 (2012).
- [13] N. D. Drummond, V. Zólyomi, and V. I. Fal’ko, “Electrically tunable band gap in silicene,” *Phys. Rev. B* **85**, 075423 (2012).
- [14] Yijun Yu, Fangyuan Yang, Xiu Fang Lu, Ya Jun Yan, Yong-Heum Cho, Liguang Ma, Xiaohai Niu, Sejoong Kim, Young-Woo Son, Donglai Feng, Shiyan Li, Sang-Wook Cheong, Xian Hui Chen, and Yuanbo Zhang, “Gate-tunable phase transitions in thin flakes of 1t-tas₂,” *Nature Nanotechnology* **10**, 270 (2015).
- [15] L. J. Li, E. C. T. O’Farrell, K. P. Loh, G. Eda, B. Özyilmaz, and A. H. Castro Neto, “Controlling many-body states by the electric-field effect in a two-dimensional material,” *Nature* **529**, 185 (2015).
- [16] Binghai Yan and Shou-Cheng Zhang, “Topological materials,” *Reports on Progress in Physics* **75**, 096501 (2012).
- [17] Yoichi Ando, “Topological insulator materials,” *Journal of the Physical Society of Japan* **82**, 102001 (2013).
- [18] Yafei Ren, Zhenhua Qiao, and Qian Niu, “Topological phases in two-dimensional materials: a review,” *Reports on Progress in Physics* **79**, 066501 (2016).
- [19] C. L. Kane and E. J. Mele, “Quantum spin Hall effect in graphene,” *Phys. Rev. Lett.* **95**, 226801 (2005).
- [20] C. L. Kane and E. J. Mele, “Z₂ topological order and the quantum spin Hall effect,” *Phys. Rev. Lett.* **95**, 146802 (2005).
- [21] D. J. Thouless, M. Kohmoto, M. P. Nightingale, and M. den Nijs, “Quantized hall conductance in a two-dimensional periodic potential,” *Phys. Rev. Lett.* **49**, 405–408 (1982).
- [22] Liang Fu, C. L. Kane, and E. J. Mele, “Topological insulators in three dimensions,” *Phys. Rev. Lett.* **98**, 106803 (2007).
- [23] Liang Fu and C. L. Kane, “Topological insulators with inversion symmetry,” *Phys. Rev. B* **76**, 045302 (2007).
- [24] J. E. Moore and L. Balents, “Topological invariants of time-reversal-invariant band structures,” *Phys. Rev. B* **75**, 121306 (2007).
- [25] Xiao-Liang Qi, Taylor Hughes, and Shou-Cheng Zhang, “Topological Field Theory of Time-Reversal Invariant Insulators,” *Phys. Rev. B* **78**, 195424 (2008).
- [26] Andreas P. Schnyder, Shinsei Ryu, Akira Furusaki, and Andreas W. W. Ludwig, “Classification of topological insulators and superconductors in three spatial dimensions,” *Phys. Rev. B* **78**, 195125 (2008).
- [27] Alexei Kitaev, “Periodic table for topological insulators and superconductors,” *AIP Conference Proceedings* **1134**, 22 (2009).
- [28] Shinsei Ryu, Andreas Schnyder, Akira Furusaki, and Andreas Ludwig, “Topological insulators and superconductors: ten-fold way and dimensional hierarchy,” *New J. Phys.* **12**, 065010 (2010).
- [29] Zhong Wang, Xiao-Liang Qi, and Shou-Cheng Zhang, “Topological order parameters for interacting topological insulators,” *Phys. Rev. Lett.* **105**, 256803 (2010).
- [30] Zhong Wang and Shou-Cheng Zhang, “Simplified topological invariants for interacting insulators,” *Phys. Rev. X* **2**, 031008 (2012).
- [31] M. Z. Hasan and C. L. Kane, “*Colloquium* : Topological insulators,” *Rev. Mod. Phys.* **82**, 3045–3067 (2010).
- [32] Xiao-Liang Qi and Shou-Cheng Zhang, “Topological insulators and superconductors,” *Rev. Mod. Phys.* **83**, 1057–1110 (2011).
- [33] A. Bansil, Hsin Lin, and Tanmoy Das, “*Colloquium* : Topological band theory,” *Rev. Mod. Phys.* **88**, 021004 (2016).
- [34] P. M. Ostrovsky, I. V. Gornyi, and A. D. Mirlin, “Interaction-induced criticality in z₂ topological insulators,” *Phys. Rev. Lett.* **105**, 036803 (2010).
- [35] Pallab Goswami and Sudip Chakravarty, “Quantum criticality between topological and band insulators in 3 + 1 dimensions,” *Phys. Rev. Lett.* **107**, 196803 (2011).
- [36] Tobias Gulden, Michael Janas, Yuting Wang, and Alex Kamenev, “Universal finite-size scaling around topological quantum phase transitions,”

- Phys. Rev. Lett. **116**, 026402 (2016).
- [37] Dmitry Bagrets, Alexander Altland, and Alex Kamenev, “Sinai diffusion at quasi-1d topological phase transitions,” Phys. Rev. Lett. **117**, 196801 (2016).
- [38] Bitan Roy, Pallab Goswami, and Jay D. Sau, “Continuous and discontinuous topological quantum phase transitions,” Phys. Rev. B **94**, 041101 (2016).
- [39] Wei Chen, Markus Legner, Andreas Rüegg, and Manfred Sigrist, “Correlation length, universality classes, and scaling laws associated with topological phase transitions,” Phys. Rev. B **95**, 075116 (2017).
- [40] Yuting Wang, Tobias Gulden, and Alex Kamenev, “Finite-size scaling of entanglement entropy in one-dimensional topological models,” Phys. Rev. B **95**, 075401 (2017).
- [41] Pallab Goswami and Sudip Chakravarty, “Superuniversality of topological quantum phase transition and global phase diagram of dirty topological systems in three dimensions,” Phys. Rev. B **95**, 075131 (2017).
- [42] Tian-Sheng Zeng, W. Zhu, Jian-Xin Zhu, and D. N. Sheng, “Nature of continuous phase transitions in interacting topological insulators,” Phys. Rev. B **96**, 195118 (2017).
- [43] M. A. Griffith and M. A. Continentino, “Casimir amplitudes in topological quantum phase transitions,” Phys. Rev. E **97**, 012107 (2018).
- [44] K v Klitzing, Gerhard Dorda, and Michael Pepper, “New method for high-accuracy determination of the fine-structure constant based on quantized hall resistance,” Physical Review Letters **45**, 494 (1980).
- [45] D. C. Tsui, H. L. Stormer, and A. C. Gossard, “Two-dimensional magnetotransport in the extreme quantum limit,” Phys. Rev. Lett. **48**, 1559–1562 (1982).
- [46] Markus König, Steffen Wiedmann, Christoph Brüne, Andreas Roth, Hartmut Buhmann, Laurens Molenkamp, Xiao-Liang Qi, and Shou-Cheng Zhang, “Quantum spin Hall insulator state in HgTe quantum wells,” Science **318**, 766–770 (2007).
- [47] Cui-Zu Chang, Jinsong Zhang, Xiao Feng, Jie Shen, Zuocheng Zhang, Minghua Guo, Kang Li, Yunbo Ou, Pang Wei, Li-Li Wang, *et al.*, “Experimental observation of the quantum anomalous hall effect in a magnetic topological insulator,” Science **340**, 167–170 (2013).
- [48] Qing Lin He, Lei Pan, Alexander L. Stern, Edward C. Burks, Xiaoyu Che, Gen Yin, Jing Wang, Biao Lian, Quan Zhou, Eun Sang Choi, Koichi Murata, Xufeng Kou, Zhijie Chen, Tianxiao Nie, Qiming Shao, Yabin Fan, Shou-Cheng Zhang, Kai Liu, Jing Xia, and Kang L. Wang, “Chiral majorana fermion modes in a quantum anomalous hall insulator–superconductor structure,” Science **357**, 294–299 (2017).
- [49] Ralph von Baltz and Wolfgang Kraut, “Theory of the bulk photovoltaic effect in pure crystals,” Phys. Rev. B **23**, 5590–5596 (1981).
- [50] V. M. Fridkin, “Bulk photovoltaic effect in noncentrosymmetric crystals,” Crystallography Reports **46**, 654–658 (2001).
- [51] J. E. Sipe and A. I. Shkrebtii, “Second-order optical response in semiconductors,” Phys. Rev. B **61**, 5337–5352 (2000).
- [52] Liang Z. Tan and Andrew M. Rappe, “Enhancement of the bulk photovoltaic effect in topological insulators,” Phys. Rev. Lett. **116**, 237402 (2016).
- [53] Shuichi Murakami, “Phase transition between the quantum spin hall and insulator phases in 3d: emergence of a topological gapless phase,” New Journal of Physics **9**, 356 (2007).
- [54] Shuichi Murakami and Shun-ichi Kuga, “Universal phase diagrams for the quantum spin hall systems,” Phys. Rev. B **78**, 165313 (2008).
- [55] Di Xiao, Ming-Che Chang, and Qian Niu, “Berry phase effects on electronic properties,” Rev. Mod. Phys. **82**, 1959–2007 (2010).
- [56] Ashley M. Cook, Benjamin M. Fregoso, Fernando de Juan, Sinsisa Coh, and Joel E. Moore, “Design principles for shift current photovoltaics,” Nat. Commun. **8**, 14176 (2017).
- [57] Steve M. Young and Andrew M. Rappe, “First principles calculation of the shift current photovoltaic effect in ferroelectrics,” Phys. Rev. Lett. **109**, 116601 (2012).
- [58] Steve M. Young, Fan Zheng, and Andrew M. Rappe, “First-principles calculation of the bulk photovoltaic effect in bismuth ferrite,” Phys. Rev. Lett. **109**, 236601 (2012).
- [59] Takahiro Morimoto and Naoto Nagaosa, “Topological nature of nonlinear optical effects in solids,” Science Advances **2** (2016), 10.1126/sciadv.1501524.
- [60] Kun Woo Kim, Takahiro Morimoto, and Naoto Nagaosa, “Shift charge and spin photocurrents in dirac surface states of topological insulator,” Phys. Rev. B **95**, 035134 (2017).
- [61] Tonatiuh Rangel, Benjamin M. Fregoso, Bernardo S. Mendoza, Takahiro Morimoto, Joel E. Moore, and Jeffrey B. Neaton, “Large bulk photovoltaic effect and spontaneous polarization of single-layer monochalcogenides,” Phys. Rev. Lett. **119**, 067402 (2017).
- [62] Benjamin M. Fregoso, Takahiro Morimoto, and Joel E. Moore, “Quantitative relationship between polarization differences and the zone-averaged shift photocurrent,” Phys. Rev. B **96**, 075421 (2017).
- [63] Chong Wang, Xiaoyu Liu, Lei Kang, Bing-Lin Gu, Yong Xu, and Wenhui Duan, “First-principles calculation of nonlinear optical responses by wannier interpolation,” Phys. Rev. B **96**, 115147 (2017).
- [64] Hiroaki Ishizuka and Naoto Nagaosa, “Local photo-excitation of shift current in noncentrosymmetric systems,” New Journal of Physics **19**, 033015 (2017).
- [65] Supplemental material.
- [66] Ion Garate, “Phonon-induced topological transitions and crossovers in dirac materials,” Phys. Rev. Lett. **110**, 046402 (2013).
- [67] Steffen Wiedmann, Andreas Jost, Cornelius Thienel, Christoph Brüne, Philipp Leubner, Hartmut Buhmann, Laurens W. Molenkamp, J. C. Maan, and Uli Zeitler, “Temperature-driven transition from a semiconductor to a topological insulator,” Phys. Rev. B **91**, 205311 (2015).
- [68] Gabriel Antonius and Steven G. Louie, “Temperature-induced topological phase transitions: Promoted versus suppressed nontrivial topology,” Phys. Rev. Lett. **117**, 246401 (2016).
- [69] Bartomeu Monserrat and David Vanderbilt, “Temperature effects in the band structure of topological insulators,” Phys. Rev. Lett. **117**, 226801 (2016).
- [70] A. M. Kadykov, S. S. Krishtopenko, B. Jouault, W. Desrat, W. Knap, S. Ruffenach, C. Consejo, J. Torres, S. V. Morozov, N. N. Mikhailov, S. A. Dvoretiskii, and F. Teppe, “Temperature-induced topological phase transition in hgte quantum wells,” Phys. Rev. Lett. **120**, 086401 (2018).
- [71] F. D. M. Haldane, “Model for a quantum hall effect without landau levels: Condensed-matter realization of the “parity anomaly,”” Phys. Rev. Lett. **61**, 2015–2018 (1988).
- [72] J. E. Moore and J. Orenstein, “Confinement-induced berry phase and helicity-dependent photocurrents,” Phys. Rev. Lett. **105**, 026805 (2010).
- [73] Inti Sodemann and Liang Fu, “Quantum nonlinear hall effect induced by berry curvature dipole in time-reversal invariant materials,” Phys. Rev. Lett. **115**, 216806 (2015).
- [74] Yang Zhang, Yan Sun, and Binghai Yan, “Berry curvature dipole in weyl semimetal materials: An ab initio study,”

- Phys. Rev. B **97**, 041101 (2018).
- [75] Cheng-Cheng Liu, Wanxiang Feng, and Yugui Yao, “Quantum spin hall effect in silicene and two-dimensional germanium,” Phys. Rev. Lett. **107**, 076802 (2011).
- [76] Cheng-Cheng Liu, Hua Jiang, and Yugui Yao, “Low-energy effective hamiltonian involving spin-orbit coupling in silicene and two-dimensional germanium and tin,” Phys. Rev. B **84**, 195430 (2011).
- [77] Yong Xu, Binghai Yan, Hai-Jun Zhang, Jing Wang, Gang Xu, Peizhe Tang, Wenhui Duan, and Shou-Cheng Zhang, “Large-gap quantum spin hall insulators in tin films,” Phys. Rev. Lett. **111**, 136804 (2013).
- [78] Motohiko Ezawa, “A topological insulator and helical zero mode in silicene under an inhomogeneous electric field,” New Journal of Physics **14**, 033003 (2012).
- [79] Alessandro Molle, Joshua Goldberger, Michel Houssa, Yong Xu, Shou-Cheng Zhang, and Deji Akinwande, “Buckled two-dimensional xene sheets,” Nature Materials **16**, 163.
- [80] Ivan Knez, Rui-Rui Du, and Gerard Sullivan, “Evidence for helical edge modes in inverted InAs/GaSb quantum wells,” Phys. Rev. Lett. **107**, 136603 (2011).
- [81] Chaoxing Liu, Taylor L. Hughes, Xiao-Liang Qi, Kang Wang, and Shou-Cheng Zhang, “Quantum spin hall effect in inverted type-ii semiconductors,” Phys. Rev. Lett. **100**, 236601 (2008).
- [82] M. Nakamura, S. Horiuchi, F. Kagawa, N. Ogawa, T. Kurumaji, Y. Tokura, and M. Kawasaki, “Shift current photovoltaic effect in a ferroelectric charge-transfer complex,” Nature Communications **8**, 281 (2017).
- [83] G. B. Osterhoudt, L. K. Diebel, M. J. Gray, X. Yang, J. Stanco, X. Huang, B. Shen, N. Ni, P. J. W. Moll, Y. Ran, and K. S. Burch, “Colossal Bulk Photovoltaic Effect in a Weyl Semimetal,” ArXiv e-prints (2017), arXiv:1712.04951 [cond-mat.mes-hall].
-

Supplemental Material

Zhongbo Yan

School of Physics, Sun Yat-sen University, Guangzhou, 510275, China

This supplemental material contains three parts: (I) The derivation of Eq.(3) in the main text; (II) Some details of the calculation of shift current tensor, and a comparison between the results from the full Hamiltonian and those from the low-energy continuum Hamiltonian; (III) Demonstration of the sign-reversal behavior of band-edge shift current tensor for spin nonconserving case.

I. THE DERIVATION OF EQ.(3) IN THE MAIN TEXT

The shift current is a second-order optical effect with the induced direct current proportional to the square of the optical field, i.e., $J_a = \sigma^{abc}(\omega)\mathcal{E}_b(\omega)\mathcal{E}_c(-\omega)$. For linearly polarized light and in the independent particle approximation, the shift current tensor σ^{abc} is given by[51]

$$\sigma^{abb}(\omega) = \frac{2\pi e^3}{\hbar} \int \frac{d^D k}{(2\pi)^D} \sum_{\alpha\beta} f_{\alpha\beta} |r_{\alpha\beta}^b|^2 R_{\alpha\beta}^a \delta(\hbar\omega - E_{\beta\alpha}), \quad (\text{S1})$$

where $r_{\alpha\beta}^a = i\langle u_\alpha | \partial_a u_\beta \rangle$ (∂_a is a shorthand notation of $\frac{\partial}{\partial k_a}$) with $\alpha \neq \beta$ is the interband Berry connection; $f_{\alpha\beta} = f_\alpha - f_\beta$ with $f_\alpha = 1/(1 + \exp[(E_\alpha(\mathbf{k}) - \mu)/k_B T])$ the Fermi-Dirac distribution function, where μ is the chemical potential, T is the temperature, and k_B is the Boltzmann constant; $E_{\beta\alpha} = E_\beta(\mathbf{k}) - E_\alpha(\mathbf{k})$ represents the energy difference between two bands labeled by α and β at momentum \mathbf{k} ; $R_{\alpha\beta}^a = -\partial_a \arg(r_{\alpha\beta}^b) + \xi_{\alpha\alpha}^a - \xi_{\beta\beta}^a$ is known as the shift vector which is related to the electric polarization between bands[62]; $\xi_{\alpha\alpha}^a = i\langle u_\alpha | \partial_a u_\alpha \rangle$ is the intraband Berry connection. Although the shift vector involves the gauge-dependent Berry connection, the formula in Eq.(S1) is gauge-invariant.

Let us focus on the two-band case. For a two-band Hamiltonian, it can always be expressed in terms of the Pauli matrices as

$$H(\mathbf{k}) = \mathbf{d}(\mathbf{k}) \cdot \boldsymbol{\tau} + \epsilon(\mathbf{k})\mathbf{I}, \quad (\text{S2})$$

where $\mathbf{d}(\mathbf{k}) = (d_x(\mathbf{k}), d_y(\mathbf{k}), d_z(\mathbf{k}))$, $\boldsymbol{\tau} = (\tau_x, \tau_y, \tau_z)$ are Pauli matrices, and \mathbf{I} is the rank-2 unit matrix. Correspondingly, the energy spectra read

$$E_\pm(\mathbf{k}) = \epsilon(\mathbf{k}) \pm d(\mathbf{k}), \quad (\text{S3})$$

and the eigenvectors take the form

$$|u_+(\mathbf{k})\rangle = \begin{pmatrix} \cos \frac{\theta_{\mathbf{k}}}{2} \\ \sin \frac{\theta_{\mathbf{k}}}{2} e^{i\phi_{\mathbf{k}}} \end{pmatrix}, \quad |u_-(\mathbf{k})\rangle = \begin{pmatrix} \sin \frac{\theta_{\mathbf{k}}}{2} e^{-i\phi_{\mathbf{k}}} \\ -\cos \frac{\theta_{\mathbf{k}}}{2} \end{pmatrix}, \quad (\text{S4})$$

where $d(\mathbf{k}) = \sqrt{\sum_{i=x,y,z} d_i(\mathbf{k})^2}$, $\theta_{\mathbf{k}} = \arctan \sqrt{d_x^2(\mathbf{k}) + d_y^2(\mathbf{k})}/d_z(\mathbf{k})$, and $\phi_{\mathbf{k}} = \arctan d_y(\mathbf{k})/d_x(\mathbf{k})$ (for brevity of notation, in this section we no longer write down the \mathbf{k} -dependence explicitly). According to the eigenvectors, the interband and intraband Berry connections are given by

$$\begin{aligned} r_{-+}^b &= i\langle u_- | \partial_b u_+ \rangle \\ &= -\frac{ie^{i\phi_{\mathbf{k}}}}{2} (\partial_b \theta_{\mathbf{k}} + i \sin \theta_{\mathbf{k}} \partial_b \phi_{\mathbf{k}}) = (r_{+-}^b)^*, \\ \xi_{--}^a &= i\langle u_- | \partial_a u_- \rangle = \sin^2 \frac{\theta_{\mathbf{k}}}{2} \partial_a \phi_{\mathbf{k}}, \\ \xi_{++}^a &= i\langle u_+ | \partial_a u_+ \rangle = -\sin^2 \frac{\theta_{\mathbf{k}}}{2} \partial_a \phi_{\mathbf{k}}. \end{aligned} \quad (\text{S5})$$

Thus, $|r_{-+}^b|^2 = [(\partial_b \theta_{\mathbf{k}})^2 + \sin^2 \theta_{\mathbf{k}} (\partial_b \phi_{\mathbf{k}})^2]/4$, and the shift vector is given by

$$\begin{aligned} R_{-+}^a &= -\partial_a \arg(r_{-+}^b) + \xi_{--}^a - \xi_{++}^a \\ &= -\partial_a \phi_{\mathbf{k}} - \partial_a \arctan \frac{\sin \theta_{\mathbf{k}} \partial_b \phi_{\mathbf{k}}}{\partial_b \theta_{\mathbf{k}}} + 2 \sin^2 \frac{\theta_{\mathbf{k}}}{2} \partial_a \phi_{\mathbf{k}} \\ &= -\cos \theta_{\mathbf{k}} \partial_a \phi_{\mathbf{k}} - \partial_a \arctan \frac{\sin \theta_{\mathbf{k}} \partial_b \phi_{\mathbf{k}}}{\partial_b \theta_{\mathbf{k}}}. \end{aligned} \quad (\text{S6})$$

By using the expression of $\theta_{\mathbf{k}}$ and $\phi_{\mathbf{k}}$, a straightforward calculation reveals

$$|r_{-+}^b|^2 = \frac{1}{8d^4} \sum_{ij} (d_i \partial_b d_j - d_j \partial_b d_i)^2. \quad (\text{S7})$$

It is readily seen that $|r_{-+}^b|^2$ is invariant under the cyclic changes, $\{d_x \rightarrow d_y, d_y \rightarrow d_z, d_z \rightarrow d_x\}$ and $\{d_x \rightarrow d_z, d_y \rightarrow d_x, d_z \rightarrow d_y\}$. Meanwhile, the shift current tensor is a physical quantity, such a cyclic change will also not affect its result. By using this cyclic property, it is straightforward to find

$$\begin{aligned} \int \cos \theta_{\mathbf{k}} \partial_a \phi_{\mathbf{k}} &= \int \frac{d_z (d_x \partial_a d_y - d_y \partial_a d_x)}{d(d_x^2 + d_y^2)} \\ &= \int \frac{d_z (d_x \partial_a d_y - d_y \partial_a d_x) + \text{cyclic changes}}{d(d_x^2 + d_y^2) + \text{cyclic changes}} \\ &= \int \frac{\mathbf{d} \cdot (\mathbf{d} \times \partial_a \mathbf{d})}{2d^3} = 0. \end{aligned} \quad (\text{S8})$$

Thus, the shift current tensor is given by

$$\begin{aligned} \sigma^{abb} &= \frac{2\pi e^3}{\hbar} \int \frac{d^D k}{(2\pi)^D} f_{-+} |r_{-+}^b|^2 R_{-+}^a \delta(\hbar\omega - 2d) \\ &= -\frac{2\pi e^3}{\hbar} \int \frac{d^D k}{(2\pi)^D} f_{-+} |r_{-+}^b|^2 (\partial_a \arctan \frac{\sin \theta_{\mathbf{k}} \partial_b \phi_{\mathbf{k}}}{\partial_b \theta_{\mathbf{k}}} + \text{cyclic changes}) \delta(\hbar\omega - 2d) \\ &= \frac{\pi e^3}{2\hbar} \int \frac{d^D k}{(2\pi)^D} \{[\sin \theta_{\mathbf{k}} \partial_b \phi_{\mathbf{k}} \partial_{ab} \theta_{\mathbf{k}} - \partial_a (\sin \theta_{\mathbf{k}} \partial_b \phi_{\mathbf{k}}) \partial_b \theta_{\mathbf{k}}] + \text{cyclic changes}\} f_{-+} \delta(\hbar\omega - 2d). \end{aligned}$$

It is noteworthy that here the ‘‘cyclic change’’ means that the nominator and denominator of $[\sin \theta_{\mathbf{k}} \partial_b \phi_{\mathbf{k}} \partial_{ab} \theta_{\mathbf{k}} - \partial_a (\sin \theta_{\mathbf{k}} \partial_b \phi_{\mathbf{k}}) \partial_b \theta_{\mathbf{k}}]$ do a simultaneous cyclic change, like that in Eq.(S8). The integrand in the bracket can be rewritten in terms of the three components of the \mathbf{d} -vector. According to the expressions of $\theta_{\mathbf{k}}$ and $\phi_{\mathbf{k}}$, it is readily found

$$\begin{aligned} \sin \theta_{\mathbf{k}} \partial_b \phi_{\mathbf{k}} &= \frac{d_x \partial_a d_y - d_y \partial_a d_x}{d \sqrt{d_x^2 + d_y^2}}, \\ \partial_b \theta_{\mathbf{k}} &= \frac{(d_x \partial_b d_x + d_y \partial_b d_y) d_z - (d_x^2 + d_y^2) \partial_b d_z}{d^2 \sqrt{d_x^2 + d_y^2}}, \end{aligned} \quad (\text{S9})$$

then

$$\begin{aligned} &\sin \theta_{\mathbf{k}} \partial_b \phi_{\mathbf{k}} \partial_{ab} \theta_{\mathbf{k}} - \partial_a (\sin \theta_{\mathbf{k}} \partial_b \phi_{\mathbf{k}}) \partial_b \theta_{\mathbf{k}} \\ &= \frac{(d_x \partial_b d_y - d_y \partial_b d_x)}{d^5 (d_x^2 + d_y^2)^2} \{d^2 (d_x^2 + d_y^2) [(\partial_a d_x \partial_b d_x + d_x \partial_{ab} d_x + \partial_a d_y \partial_b d_y + d_y \partial_{ab} d_y) d_z + (d_x \partial_b d_x + d_y \partial_b d_y) \partial_a d_z \\ &\quad - 2(d_x \partial_a d_x + d_y \partial_a d_y) \partial_b d_z - (d_x^2 + d_y^2) \partial_{ab} d_z] - 2(d_x^2 + d_y^2) [(d_x \partial_b d_x + d_y \partial_b d_y) d_z - (d_x^2 + d_y^2) \partial_b d_z] \\ &\quad \times (d_x \partial_a d_x + d_y \partial_a d_y + d_z \partial_a d_z) - d^2 [(d_x \partial_b d_x + d_y \partial_b d_y) d_z - (d_x^2 + d_y^2) \partial_b d_z] (d_x \partial_a d_x + d_y \partial_a d_y)\} \\ &\quad - \frac{[(d_x \partial_b d_x + d_y \partial_b d_y) d_z - (d_x^2 + d_y^2) \partial_b d_z]}{d^5 (d_x^2 + d_y^2)^2} \{d^2 (d_x^2 + d_y^2) (\partial_a d_x \partial_b d_y + d_x \partial_{ab} d_y - \partial_a d_y \partial_b d_x - d_y \partial_{ab} d_x) \\ &\quad - (d_x^2 + d_y^2) (d_x \partial_b d_y - d_y \partial_b d_x) (d_x \partial_a d_x + d_y \partial_a d_y + d_z \partial_a d_z) - d^2 (d_x \partial_b d_y - d_y \partial_b d_x) (d_x \partial_a d_x + d_y \partial_a d_y)\}. \end{aligned} \quad (\text{S10})$$

We first consider the terms with second derivative, which give

$$\begin{aligned}
P_1 &= \frac{1}{d^5(d_x^2 + d_y^2)^2} \{ d^2(d_x^2 + d_y^2)(d_x \partial_b d_y - d_y \partial_b d_x) [(d_x \partial_{ab} d_x + d_y \partial_{ab} d_y) d_z - (d_x^2 + d_y^2) \partial_{ab} d_z] \\
&\quad - d^2(d_x^2 + d_y^2)(d_x \partial_{ab} d_y - d_y \partial_{ab} d_x) [(d_x \partial_b d_x + d_y \partial_b d_y) d_z - (d_x^2 + d_y^2) \partial_b d_z] \} \\
&= \frac{1}{d^3(d_x^2 + d_y^2)} \{ (d_x^2 + d_y^2) [(d_x \partial_{ab} d_y - d_y \partial_{ab} d_x) \partial_b d_z - (d_x \partial_b d_y - d_y \partial_b d_x) \partial_{ab} d_z] \\
&\quad + [(d_x \partial_b d_y - d_y \partial_b d_x)(d_x \partial_{ab} d_x + d_y \partial_{ab} d_y) - (d_x \partial_{ab} d_y - d_y \partial_{ab} d_x)(d_x \partial_b d_x + d_y \partial_b d_y)] d_z \} \\
&= \frac{1}{d^3} [(d_x \partial_{ab} d_y - d_y \partial_{ab} d_x) \partial_b d_z - (d_x \partial_b d_y - d_y \partial_b d_x) \partial_{ab} d_z + (\partial_{ab} d_x \partial_b d_y - \partial_{ab} d_y \partial_b d_x) d_z] \\
&= \frac{1}{d^3} [d_x (\partial_{ab} d_y \partial_b d_z - \partial_{ab} d_z \partial_b d_y) + d_y (\partial_{ab} d_z \partial_b d_x - \partial_{ab} d_x \partial_b d_z) + d_z (\partial_{ab} d_x \partial_b d_y - \partial_{ab} d_y \partial_b d_x)] \\
&= \frac{\mathbf{d} \cdot (\partial_{ab} \mathbf{d} \times \partial_b \mathbf{d})}{d^3}.
\end{aligned} \tag{S11}$$

It is apparent that such a form is invariant under the cyclic change. Thus, the contribution of this part to the shift current tensor is

$$\begin{aligned}
&\frac{\pi e^3}{2\hbar} \int \frac{d^D k}{(2\pi)^D} \frac{\mathbf{d} \cdot (\partial_{ab} \mathbf{d} \times \partial_b \mathbf{d})}{d^3} f_{-+} \delta(\hbar\omega - 2d) \\
&= \frac{\pi e^3}{2\hbar} \int \frac{d^D k}{(2\pi)^D} \frac{\mathbf{d} \cdot (\partial_{ab} \mathbf{d} \times \partial_b \mathbf{d})}{(\hbar\omega/2)^3} f_{-+} \delta(\hbar\omega - 2d) \\
&= \frac{4\pi e^3}{\hbar^4 \omega^3} \int \frac{d^D k}{(2\pi)^D} \mathbf{d} \cdot (\partial_{ab} \mathbf{d} \times \partial_b \mathbf{d}) f_{-+} \delta(\hbar\omega - 2d) \\
&= \sigma_{\Gamma}^{abb}.
\end{aligned} \tag{S12}$$

For the remaining parts, by using the cyclic change of \mathbf{d} -vector and doing some lengthy but straightforward calculations, we find the result is

$$\begin{aligned}
P_2 &= \frac{1}{d^5} \left[\sum_{ijk} \epsilon^{ijk} d_j^2 \partial_a d_i \partial_b d_j \partial_b d_k + \sum_{ijk} \epsilon^{ijk} d_i d_j \partial_b d_i (\partial_a d_i \partial_b d_k - \partial_b d_i \partial_a d_k) \right] \\
&= \frac{1}{d^5} \left[\sum_{ijk} \epsilon^{ijk} d_j \partial_a d_i \partial_b d_k (d_i \partial_b d_i + d_j \partial_b d_j) - \sum_{ijk} \epsilon^{ijk} d_j \partial_a d_k (d_i \partial_b d_i) \right] \\
&= \frac{1}{d^5} \left[\sum_{ijk} \epsilon^{ijk} d_j \partial_a d_i \partial_b d_k (d_i \partial_b d_i + d_j \partial_b d_j) - \sum_{ijk} \epsilon^{kji} d_j \partial_b d_k \partial_a d_i (d_k \partial_b d_k) \right] \\
&= \frac{1}{d^5} \left[\sum_{ijk} \epsilon^{ijk} d_j \partial_a d_i \partial_b d_k (d_i \partial_b d_i + d_j \partial_b d_j + d_k \partial_b d_k) \right] \\
&= \frac{1}{d^5} \left[\sum_{ijk} \epsilon^{ijk} d_j \partial_a d_i \partial_b d_k (d \partial_b d) \right] \\
&= \frac{1}{d^4} \left[\sum_{ijk} \epsilon^{ijk} d_j \partial_a d_i \partial_b d_k (\partial_b d) \right] \\
&= -\frac{1}{d^4} [\mathbf{d} \cdot (\partial_a \mathbf{d} \times \partial_b \mathbf{d}) (\partial_b d)] \\
&= \frac{2}{d} \Omega_{ab} (\partial_b d),
\end{aligned} \tag{S13}$$

where $\Omega_{ab} = -\mathbf{d} \cdot (\partial_a \mathbf{d} \times \partial_b \mathbf{d}) / 2d^3$ is the Berry curvature of the valence band. The contribution of this part to the shift current

tensor is

$$\begin{aligned}
& \frac{\pi e^3}{2\hbar} \int \frac{d^D k}{(2\pi)^D} \frac{2\Omega_{ab}(\partial_b d)}{d} f_{-+} \delta(\hbar\omega - 2d) \\
&= \frac{\pi e^3}{2\hbar} \int \frac{d^D k}{(2\pi)^D} \frac{2\Omega_{ab}(\partial_b d)}{\hbar\omega/2} f_{-+} \delta(\hbar\omega - 2d) \\
&= \frac{2\pi e^3}{\hbar^2 \omega} \int \frac{d^D k}{(2\pi)^D} \Omega_{ab}(\partial_b d) f_{-+} \delta(\hbar\omega - 2d) \\
&= \sigma_{\text{II}}^{abb}.
\end{aligned} \tag{S14}$$

The summation of σ_{I}^{abb} and σ_{II}^{abb} gives the formula in Eq.(3) of the main text.

II. SHIFT CURRENT TENSOR OF THE LOW-ENERGY CONTINUUM HAMILTONIAN

In momentum space, the Kane-Mele model is given by $H = \sum_{\mathbf{k}} c_{\mathbf{k}}^\dagger H(\mathbf{k}) c_{\mathbf{k}}$ with $c_{\mathbf{k}} = (c_{A,\mathbf{k}\uparrow}, c_{B,\mathbf{k}\uparrow}, c_{A,\mathbf{k}\downarrow}, c_{B,\mathbf{k}\downarrow})^T$ and

$$\begin{aligned}
H(\mathbf{k}) &= 2\lambda_{\text{so}} \left(2 \sin \frac{\sqrt{3}k_x a}{2} \cos \frac{3k_y a}{2} - \sin \sqrt{3}k_x a \right) \tau_z s_z \\
&+ \lambda_v \tau_z + t \left(\cos k_y a + 2 \cos \frac{\sqrt{3}k_x a}{2} \cos \frac{k_y a}{2} \right) \tau_x \\
&+ t \left(\sin k_y a - 2 \cos \frac{\sqrt{3}k_x a}{2} \sin \frac{k_y a}{2} \right) \tau_y,
\end{aligned} \tag{S15}$$

where τ_i with $i = \{x, y, z\}$ are Pauli matrices acting on the sublattice space, and s_z is a Pauli matrix acting on the spin space. For brevity of notation, below we set the lattice constant $a = 1$ unless otherwise specified. For this model, the band edges are located at the two points $\mathbf{K} = (-\frac{4\pi}{3\sqrt{3}}, 0)$ and $\mathbf{K}' = (\frac{4\pi}{3\sqrt{3}}, 0)$. By expanding the full Hamiltonian in Eq.(S15) around these two points to second order in momentum, the low-energy continuum Hamiltonian is given by $H(\mathbf{q}) = \sum_{\chi, s} \oplus \mathbf{d}_{\chi, s}(\mathbf{q}) \cdot \boldsymbol{\tau}$ with

$$\begin{aligned}
d_{\chi, s; x}(\mathbf{q}) &= \frac{3t}{2} (\chi q_x + \frac{1}{4} q_x^2 - \frac{1}{4} q_y^2), \\
d_{\chi, s; y}(\mathbf{q}) &= \frac{3t}{2} (q_y - \frac{1}{2} \chi q_x q_y), \\
d_{\chi, s; z}(\mathbf{q}) &= -3\sqrt{3}\lambda_{\text{so}} \chi s [1 - \frac{3}{4} (q_x^2 + q_y^2)] + \lambda_v,
\end{aligned} \tag{S16}$$

where $\chi = +1$ for K valley, $\chi = -1$ for K' valley, $s = +1$ for up spin and $s = -1$ for down spin. For the energy spectra, we also keep the momentum to second order,

$$E_{\chi, s; \pm}(\mathbf{q}) = \pm d_{\chi, s}(\mathbf{q}) = \pm \sqrt{\frac{9\eta_{\chi, s} t^2}{4} (q_x^2 + q_y^2) + m_{\chi, s}^2}, \tag{S17}$$

where $m_{\chi, s} = -3\sqrt{3}\lambda_{\text{so}}\chi s + \lambda_v$, and $\eta_{\chi, s} = 1 + 2\sqrt{3}\lambda_{\text{so}}m_{\chi, s}\chi s/t^2$. For this low-energy continuum Hamiltonian, we will consider $t \gg \lambda_{\text{so}}, \lambda_v$ so that $\eta_{\chi, s}$ is always positive definite and the band edges are indeed located at the two points \mathbf{K} and \mathbf{K}' .

A short calculation reveals

$$\begin{aligned}
F_{1; \chi, s}^{yyy} &= \mathbf{d}_{\chi, s}(\mathbf{q}) \cdot (\partial_{yy} \mathbf{d}_{\chi, s}(\mathbf{q}) \times \partial_y \mathbf{d}_{\chi, s}(\mathbf{q})) \\
&= \frac{9t^2}{8} (3\sqrt{3}\lambda_{\text{so}}\chi s - \lambda_v) + \mathcal{O}(\mathbf{q}).
\end{aligned} \tag{S18}$$

Near the band edge, all higher order terms contained in $\mathcal{O}(\mathbf{q})$ can be safely neglected as $\mathbf{q} \rightarrow 0$. For frequency close to the band

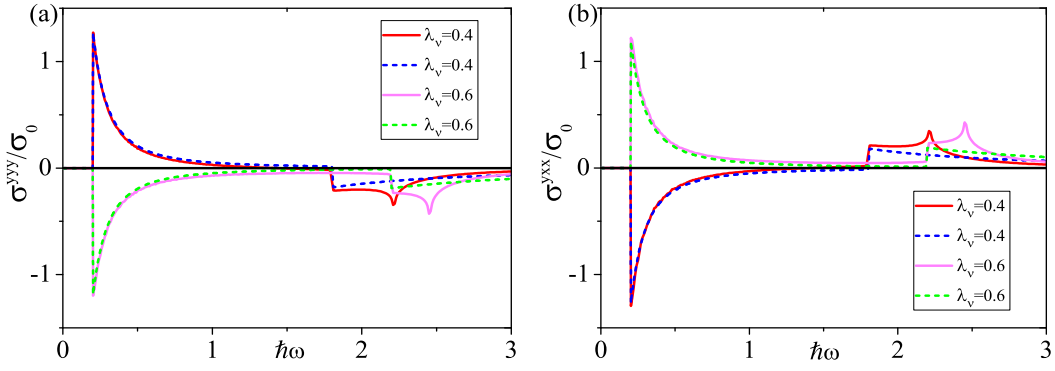


FIG. S1. The solid lines refer to shift current tensors obtained from the full lattice Hamiltonian, while the dashed lines refer to shift current tensors obtained from the low-energy continuum Hamiltonian. Parameters $t = 1$, $\lambda_{so} = \sqrt{3}/18$, (a) $\lambda_v = 0.4$, and (b) $\lambda_v = 0.6$. The chemical potential μ and temperature T are fixed to zero, correspondingly, $\sigma_0 = e^3 a / \hbar$. For the parameters chosen, there is a critical point at $\lambda_v = 0.5$.

gap,

$$\begin{aligned}
\sigma_{\chi,s}^{yyyy}(\omega) &\simeq \frac{4\pi e^3}{\hbar^4 \omega^3} \int \frac{d^2 q}{(2\pi)^2} \frac{9t^2}{8} (3\sqrt{3}\lambda_{so}\chi s - \lambda_v) \delta(\hbar\omega - 2\sqrt{\frac{9\eta_{\chi,s} t^2}{4}(q_x^2 + q_y^2) + m_{\chi,s}^2}) \\
&= \frac{e^3}{2\hbar^4 \eta_{\chi,s} \omega^3} \int_0^\infty dx (3\sqrt{3}\lambda_{so}\chi s - \lambda_v) \delta(\hbar\omega - 2\sqrt{x + m_{\chi,s}^2}) \\
&= \frac{e^3}{4\hbar^3 \eta_{\chi,s} \omega^2} (3\sqrt{3}\lambda_{so}\chi s - \lambda_v) \Theta(\hbar\omega - 2|m_{\chi,s}|) \\
&= -\frac{e^3 m_{\chi,s}}{4\hbar^3 \eta_{\chi,s} \omega^2} \Theta(\hbar\omega - 2|m_{\chi,s}|).
\end{aligned} \tag{S19}$$

For the off-diagonal component, we find

$$\begin{aligned}
F_{1;\chi,s}^{yxx} &= \mathbf{d}_{\chi,s}(\mathbf{q}) \cdot (\partial_{yx} \mathbf{d}_{\chi,s}(\mathbf{q}) \times \partial_x \mathbf{d}_{\chi,s}(\mathbf{q})) \\
&= -\frac{9t^2}{8} (3\sqrt{3}\lambda_{so}\chi s - \lambda_v) + \mathcal{O}(\mathbf{q}), \\
F_{2;\chi,s}^{yxx} &= (\hbar\omega)^2 \Omega_{\chi,s;yx} \partial_x d_{\chi,s} / 2 = \mathcal{O}(\mathbf{q}).
\end{aligned}$$

Again, the terms contained in $\mathcal{O}(\mathbf{q})$ can be safely neglected near the band edge. Thus for frequency close to the band gap,

$$\begin{aligned}
\sigma_{\chi,s}^{yxx}(\omega) &\simeq \frac{4\pi e^3}{\hbar^4 \omega^3} \int \frac{d^2 q}{(2\pi)^2} \left[-\frac{9t^2}{8} (3\sqrt{3}\lambda_{so}\chi s - \lambda_v) \right] \delta(\hbar\omega - 2\sqrt{\frac{9\eta_{\chi,s} t^2}{4}(q_x^2 + q_y^2) + m_{\chi,s}^2}) \\
&= -\frac{e^3}{4\hbar^3 \eta_{\chi,s} \omega^2} (3\sqrt{3}\lambda_{so}\chi s - \lambda_v) \Theta(\hbar\omega - 2|m_{\chi,s}|) \\
&= \frac{e^3 m_{\chi,s}}{4\hbar^3 \eta_{\chi,s} \omega^2} \Theta(\hbar\omega - 2|m_{\chi,s}|) \\
&\simeq -\sigma_{\chi,s}^{yyyy}(\omega).
\end{aligned} \tag{S20}$$

If we restore the lattice constant, simple dimensional analysis reveals

$$\begin{aligned}
\sigma_{\chi,s}^{yxx}(\omega) &\simeq -\sigma_{\chi,s}^{yyyy}(\omega) \\
&\simeq -\frac{e^3 a}{4\hbar^3 \eta_{\chi,s} \omega^2} (3\sqrt{3}\lambda_{so}\chi s - \lambda_v) \Theta(\hbar\omega - 2|m_{\chi,s}|).
\end{aligned}$$

We present the results from the full Hamiltonian and those from the low-energy continuum Hamiltonian in Fig.S1 for a comparison. In the figure, the solid lines refer to shift current tensors of the full Hamiltonian, and the dashed lines refer to shift current tensors of the low-energy continuum Hamiltonian under the same parameter condition, it is remarkable that although

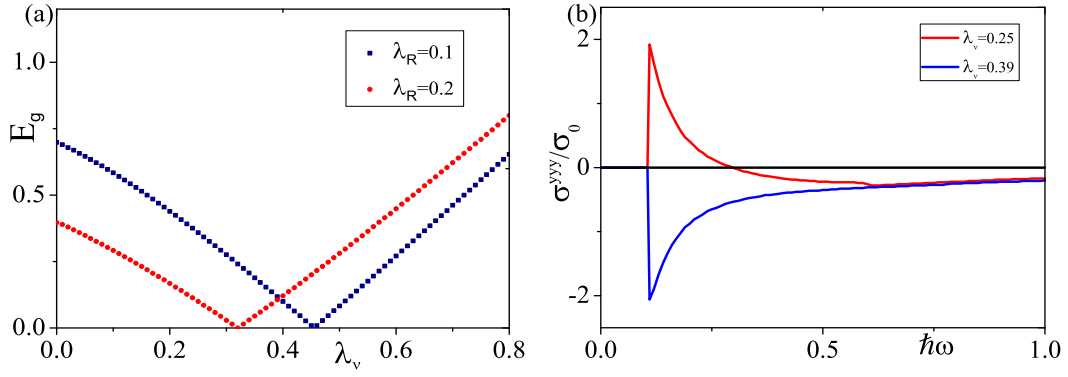


FIG. S2. Common parameters $t = 1$, $\lambda_{\text{so}} = \sqrt{3}/18$. (a) The variation of band gap with λ_v for fixed Rashba spin-orbit coupling. The gap closing points ($E_g = 0$) correspond to the critical points of TPTs. (b) Parameters $\mu = 0$, $T = 0$, $\lambda_R = 0.2$ and $\sigma_0 = e^3/\hbar$. According to the band gap evolution in (a), the TPT takes place at $\lambda_v = 0.32$. Clearly, the band-edge shift current tensor reverses its sign across the TPT, confirming that the sign-reversal behavior of band-edge shift current tensor holds no matter whether the spin is conserved or not.

only leading order terms are kept for the shift current tensors of the low-energy continuum Hamiltonian, the results from the full Hamiltonian and those from the low-energy continuum Hamiltonian agree with each other very well in a considerably broad range.

III. SPIN NON-CONSERVING CASE

In this section, we demonstrate that the sign-reversal behavior of band-edge shift current tensor holds even when the spin in the Kane-Mele model no longer conserves. For concreteness, we introduce the Rashba spin-orbit coupling to break the spin conservation, which is given by

$$H_R = i\lambda_R \sum_{\langle i,j \rangle} c_i^\dagger (\mathbf{s} \times \hat{\mathbf{d}}_{ij})_z c_j, \quad (\text{S21})$$

where $\hat{\mathbf{d}}_{ij}$ denotes the unit vector connecting i and j . Then the full Hamiltonian in momentum space becomes

$$\begin{aligned} H(\mathbf{k}) = & 2\lambda_{\text{so}} \left(2 \sin \frac{\sqrt{3}k_x a}{2} \cos \frac{3k_y a}{2} - \sin \sqrt{3}k_x a \right) \tau_z s_z + \lambda_v \tau_z + t \left(\cos k_y a + 2 \cos \frac{\sqrt{3}k_x a}{2} \cos \frac{k_y a}{2} \right) \tau_x \\ & + t \left(\sin k_y a - 2 \cos \frac{\sqrt{3}k_x a}{2} \sin \frac{k_y a}{2} \right) \tau_y - \lambda_R \left(\cos \frac{\sqrt{3}k_x a}{2} \sin \frac{k_y a}{2} + \sin k_y a \right) \tau_x s_x \\ & + \sqrt{3}\lambda_R \sin \frac{\sqrt{3}k_x a}{2} \cos \frac{k_y a}{2} \tau_x s_y + \lambda_R \left(\cos \frac{\sqrt{3}k_x a}{2} \cos \frac{k_y a}{2} - \cos k_y a \right) \tau_y s_x \\ & + \sqrt{3}\lambda_R \sin \frac{\sqrt{3}k_x a}{2} \sin \frac{k_y a}{2} \tau_y s_y. \end{aligned} \quad (\text{S22})$$

This rank-4 matrix can not be decomposed as the direct sum of two rank-2 matrices any more, so we have to use the general formula in Eq.(S1) and calculate the shift current tensor numerically. Meanwhile, as the Rashba spin-orbit coupling does not break the mirror symmetry about the $k_x = 0$ plane, σ^{xxx} and σ^{xyy} still vanish identically.

The numerical results are presented in Fig.S2. Fig.S2(a) shows that the introduction of Rashba spin-orbit coupling will change the position of critical point. Fig.S2(b) demonstrates that the sign-reversal behavior of band-edge shift current holds even when the spin conservation is broken by the Rashba spin-orbit coupling. Because we find that $\sigma^{yyy} \simeq -\sigma^{yxx}$ still holds, here only σ^{yyy} is presented.